CDF note 11199

Measurement of D^+-meson production cross section at low transverse momentum in $p\bar{p}$ collisions at $\sqrt{s} = 1.96\,\mathbf{TeV}$

The CDF Collaboration
URL http://www-cdf.fnal.gov

(Dated: June 30, 2016)

We report on a measurement of the D^+-meson production cross section as a function of transverse momentum in proton-antiproton collisions at 1.96 TeV center-of-mass energy, using the full data set collected by the CDF experiment in Tevatron Run II, and corresponding to 10 fb^{-1} of integrated luminosity. We use $D^+ \to K^-\pi^+\pi^+$ decays fully reconstructed in the central rapidity region $|y| < 1$ with transverse momentum extending down to $p_T \approx 1.5$ GeV/c, a range unexplored in proton-antiproton collisions. Events are selected online using minimally biasing requirements and an optimization is used to determine the offline selection. A two-dimensional simultaneous fit of the $K^-\pi^+\pi^+$-mass and D^+ transverse impact-parameter distributions allows determining a signal of 2950 D^+ decays produced directly in the hard scattering. The total cross section is $\sigma(D^+, p_T > 1.5\ \text{GeV}/c, |y| < 1) = 71.9 \pm 6.8(\text{stat}) \pm 9.3(\text{syst})\ \mu\text{b}$. The results agree with earlier determinations at higher transverse momentum in the region where data overlap. While the measurements lie within the band of theoretical uncertainty, differences in shape suggest that theoretical predictions can benefit by further refinement taking account these results.

Measurements of cross sections for the production of hadrons containing bottom or charm quarks (heavy-flavors) in hadron collisions offer essential information to test and refine phenomenological models of the strong interaction at small transferred four-momenta, a regime in which perturbative expansions are challenging. In addition, in searches for astrophysical neutrinos, charm production cross-sections allow for improved estimations of background rates from neutrinos produced in decays of charm hadrons from cosmic-ray interactions with atmospheric nuclei [1].

The first studies of heavy-flavor production in hadron collisions, performed at the Tevatron proton-antiproton ($p\bar{p}$) collider in 1992–1996 [2], yielded cross sections significantly larger than the predicted values [3] and prompted a dedicated effort in refining calculations [4], which resulted in reduced discrepancies. The program continued in Tevatron Run II (2001–2011) with measurements of charm-meson cross sections using $p\bar{p}$ collisions at $\sqrt{s} = 1.96$ TeV [5]. Since 2010, CERN's LHC pp collider has replaced the Tevatron as the most prolific charm-meson source, allowing the ALICE and LHCb experiments to report measurements of charm cross sections at $\sqrt{s} = 2.76$–13.00 TeV [6].

Measurements based on $p\bar{p}$ collisions, and probing different collision energies, remain essential to extend the comprehension of quantum chromodynamics (QCD) because differing admixtures of parton-level processes contribute at different energies and initial states. Previous measurements in $p\bar{p}$ collisions [5] were restricted to mesons with transverse momentum, the momentum component in the plane transverse to the beam, $p_T > 6.0$ GeV/c, because of the final-state-particle transverse-momentum thresholds used in the online event selection (trigger). Extending the reach to lower p_T, hence further into the nonperturbative regime, provides novel and unique constraints to improve QCD phenomenological models.

In this paper, we report on a measurement of cross section for D^+ mesons whose p_T extends down to 1.5 GeV/c, a range unexplored in $p\bar{p}$ collisions so far, and unlikely to be explored in the foreseeable future. The measurement is conducted as a function of meson transverse momentum using $D^+ \to K^-\pi^+\pi^+$ decays reconstructed in the full CDF Run II data set. Charge-conjugate decays are implied throughout. Events are collected through minimal, if any, requirements on the event features, thus reducing biases to the physics properties of the collected charm decays. The sample is divided into subsamples according to the D^+ candidate p_T (p_T bins). In each, we apply a data-driven optimization of the offline selection and perform a two-dimensional simultaneous fit of the resulting distributions of $K^-\pi^+\pi^+$-mass and D^+ transverse impact-parameter, the minimum transverse distance between the D^+ trajectory and the beam. The fit determines, for each p_T bin, the signal yield of D^+ candidates genuinely produced in the $p\bar{p}$ interaction or originated from excited charm resonances (primary D^+) by statistically subtracting D^+ candidates originated from b-hadron decays (secondary D^+). Each primary yield is combined with corresponding reconstruction and selection efficiencies derived using simulation to determine the cross section,

$$\sigma_i = \frac{N_i/2}{\int \mathcal{L}dt \cdot \epsilon_i \cdot \mathcal{B}}, \tag{1}$$

where N_i is the observed number of primary D^+ and D^- mesons in each p_T bin. The factor 1/2 is included because both D^+ and D^- mesons contribute to N_i and we report results solely for D^+, assuming flavor-symmetric production of charm quarks in the strong proton-antiproton interaction. The integrated luminosity $\int \mathcal{L}dt$ is normalized to an inelastic cross section of $\sigma_{p\bar{p}} = 60.7 \pm 2.4$ mb [7] and ϵ_i is the global detection, reconstruction, and selection efficiency. The branching fraction of the $D^+ \to K^-\pi^+\pi^+$ decay used is $\mathcal{B} = (9.46 \pm 0.24)\%$ [8].

The CDF II detector is a multipurpose magnetic spectrometer surrounded by calorimeters and muon detectors. The detector components relevant for this analysis are outlined as follows; a detailed description is in Ref. [9] and references therein. A silicon microstrip vertex detector and a cylindrical open-cell drift chamber immersed in a nearly uniform, 1.4 T axial magnetic field allow for the reconstruction of charged-particle trajectories (tracks) in the pseudorapidity range $|\eta| < 1$. The vertex detector contains seven concentric layers of single- and double-sided silicon sensors at radii between 1.5 and 22 cm, each providing a position measurement with up to 15 (70) μm resolution in the azimuthal (proton-beam) direction [10]. The drift chamber has 96 measurement layers, located between 40 and 137 cm in radius, organized into alternating axial and $\pm 2^\circ$ stereo superlayers [11]. The component of a charged-particle momentum transverse to the beam (p_T) is determined with a resolution of $\sigma_{p_T}/p_T^2 \approx 0.07\%$ (GeV/c)$^{-1}$, corresponding to a typical mass resolution of 6.0 MeV/c^2 for a $D^+ \to K^-\pi^+\pi^+$ decay. Gas Cherenkov detectors (CLC) covering the symmetric regions at small polar angle around the interaction region $3.7 < |\eta| < 4.7$ are used to detect hard-scatter interactions and measure luminosity [12]. CDF has a three-level trigger system. We use events collected by the zero- and minimum-bias triggers, which are designed to collect events while introducing minimum, if any, bias in the properties of the particles produced in the collision. The zero-bias trigger applies no requirements and accepts a 10^{-6} fraction (prescale factor) of $p\bar{p}$ crossings, randomly chosen. At the first trigger level, the minimum-bias trigger accepts a 10^{-5} prescale fraction of the events in which a time-coincidence between signals in the CLC at opposite sides of the interaction region is detected, which enriches the sample in $p\bar{p}$ crossings that yield inelastic interactions. At the second (third) trigger level, the minimum-bias trigger apply no requirements and accept events with 3 (1) Hz maximum rates. The large prescale factors and accept-rate reductions avoid saturation of the trigger bandwidth.

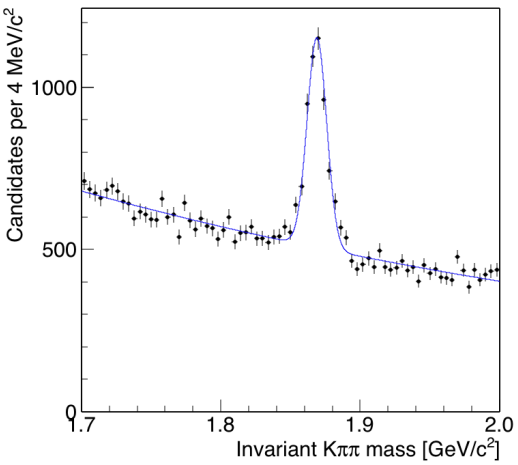

FIG. 1: Distribution of $K^-\pi^+\pi^-$ mass for the whole sample with fit overlaid.

.

The resulting samples contain 183 million zero-bias and 133 million minimum-bias events. Of these, 409 events are common to both samples and used only once in the analysis.

The offline reconstruction of signal candidates is solely based on tracking information, without using particle identification, the odd-charge particle being assigned the kaon mass. Three good-quality tracks, associated with drift-chamber and silicon-detector information and consistent with a $K^-\pi^+\pi^+$ decay, are combined in a kinematic fit to a common decay vertex to form a D^+ signal candidate. Additional criteria are applied on the vertex-fit quality, minimum azimuthal separation of any pair of signal tracks, product of their impact parameters (the minimum distance of approach of a particle trajectory to the beam), and minimum value of D^+ transverse decay-length projected onto its p_T, L_{xy}. These are fully efficient on signal and reduce backgrounds from combinations of random charged particles (combinatorial background). No more than one candidate is reconstructed in each event. We further improve the signal-to-background ratio by optimizing the selection. This is done separately for events restricted to each of the five ranges (bins) in D^+ candidate p_T 1.5–2.5, 2.5–3.5, 3.5–4.5, 4.5–6.5, and 6.5–14.5 GeV/c. First, we apply an upper threshold on the impact parameter of the D^+ candidates. This suppresses secondary D^+ candidates, which are less likely to point-back to the $p\bar{p}$ vertex because of the combined effect of the long lifetime of b hadrons and the energy released in their decay. This requirement is only applied for the optimization, but is lifted in further analysis, where the D^+ impact-parameter distribution is fit to separate statistically the signal of primary D^+ candidates from the secondaries. Then we divide the sample randomly into two subsamples. In each, we conduct an independent optimization by maximizing the quantity $S/\sqrt{S+B}$ over 1 000 possible configurations of requirements on the minimum p_T of any two final-state particles, minimum L_{xy}, and maximum value of the vertex-fit χ^2. The signal (background) S (B) yields are estimated by fits of the $K^-\pi^+\pi^+$ mass distributions with a Gaussian model for the signal and a smooth empirical function for the background. Finally, the optimal configuration resulting from a subsample is applied on the complementary subsample. Because the optimization uses the very data of the measurement, it is free from effects due to simulation mismodelings. Biased configurations due to statistical fluctuations are avoided by crossing the selections between the two independent subsamples. The optimized criteria are $p_T > 0.6-1.1$ GeV/c, $L_{xy} > 600-700$ μm, and $\chi^2 < 2-7$, depending on subsample and p_T bin. The $K^-\pi^+\pi^+$ mass distribution of the resulting sample, summed across p_T bins, is shown in Fig. 1. The sample is dominated by a background of random combinations of charged particles that accidentally meet the selection requirements (combinatorics), which has a smooth distribution and a prominent narrow peak of approximately 3400 $D^+ \to K^-\pi^+\pi^+$ decays, comprising both primary signal and secondary charm candidates. In each p_T bin, we determine the yield of primary D^+ decays using a simultaneous maximum-likelihood fit to the unbinned distributions of $K^-\pi^+\pi^+$ mass, to separate D^+ decays from combinatorics, and D^+ impact parameter, to separate primary from secondary D^+ decays. The fit model is a linear combination of probability density functions (pdf) for primary D^+ signal, secondary D^+, and combinatorial background, each consisting of the product of mass and impact-parameter pdfs. In mass, primary and secondary components are modeled jointly with a Gaussian function determined from simulation; the background pdf is a second-order polynomial function derived empirically from the D^+ mass sidebands. In impact parameter, the primary (secondary) component is modeled with the sum of three narrow (broad) Gaussian distributions determined using simulation whereas the background is modeled with a combination of Gaussian shapes that empirically reproduce the impact-parameter distribution of

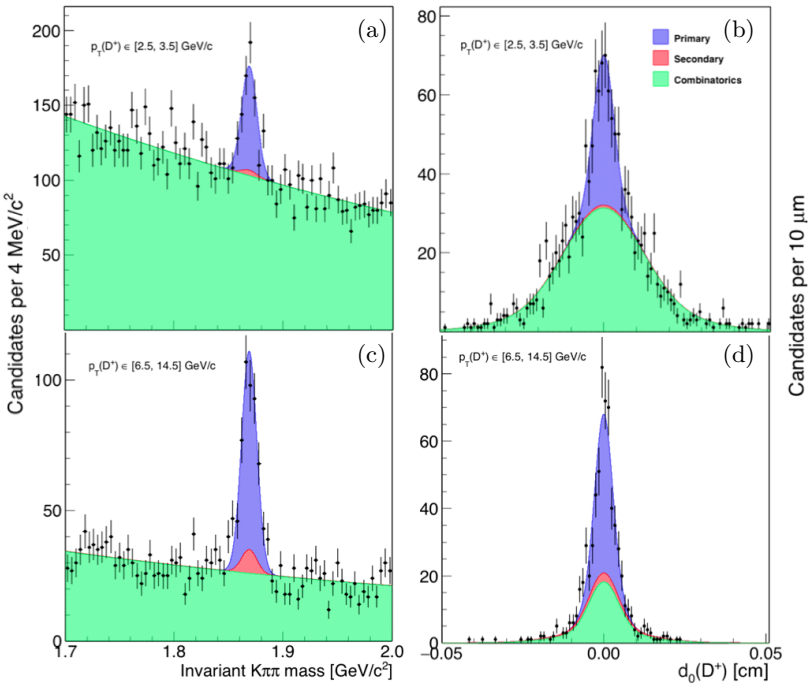

FIG. 2: Distributions of (a) $K^-\pi^+\pi^-$ mass for candidates with $2.5 < p_T < 3.5$ GeV/c and (b) D^+ impact parameter for those candidates, further restricted to have $K^-\pi^+\pi^-$ mass within three standard deviations from the peak value. Fits are overlaid. Panels (c) and (d) show the same distributions for candidates with $6.5 < p_T < 14.5$ GeV/c.

events with D^+ mass in the ranges 1.7–1.8 or 1.9–2.0 GeV/c^2 (sideband regions). The only free parameters in the fit are the numbers of primary D^+ (signal) decays and secondary D^+ decays. Tests on simplified simulated experiments show that the fit estimates are unbiased and have proper Gaussian uncertainties. Figure 2 reports examples of fits in two p_T bins. A total signal of approximately 2950 primary D^+ decays is obtained. The observed fraction of secondary decays is typically 15% of the total D^+ yield but varies between 0% and 40% depending on p_T with large uncertainties. We vary the parameters and assumptions of the signal and background models and attribute systematic uncertainties on primary signal yields in the range 0.9%–1.5%, depending on the p_T of the candidates.

We factorize the detection and reconstruction efficiency ϵ_i in each p_T-bin i in the product of trigger efficiency, offline efficiency for reconstructing three tracks that meet the quality and fiducial requirements in the drift chamber, offline efficiency for assigning the information from the silicon detector to these tracks, and the efficiency of the offline selection requirements. The only relevant effect for the zero-bias trigger efficiency is deadtime incurred in the data-acquisition system, which is already accounted for in the determination of the integrated luminosity, resulting in 100% relative efficiency. The minimum-bias trigger efficiency is determined to be (98.8 ± 0.4)% from the ratio of D^+ signal yields observed in zero-bias events that meet, or fail, the minimum-bias requirements. All offline efficiencies are reproduced accurately by the simulation [13] except for the term associated with the silicon detector. We therefore use efficiencies derived from the simulation as input for the measurement and use control samples of data to obtain systematic uncertainties that cover any potential data-simulation discrepancy in the silicon-related efficiency. Offline efficiencies ranging from 0.27% to 7.5% are determined from simulated events containing $D^+ \to K^-\pi^+\pi^+$ decays, in which distributions are weighted so that the multiplicity of primary vertices reproduces the one observed in data. Control samples of probe muons from $J/\psi \to \mu^+\mu^-$ decays and low-momentum pions from $D^{*+} \to D^0(\to K^-\pi^+)\pi^+$ decays, in which only drift-chamber information is used to select and reconstruct the probe particle, are used to determine silicon efficiencies as functions of probe-particle p_T and data-taking time from the fraction of probe particles that also meet the silicon requirements. The results are compared with silicon efficiencies determined in simulation, and the maximum observed deviation, 3.7%, is used as per-track systematic uncertainty, resulting in a 11.5% uncertainty in all D^+ transverse momentum bins. This is the largest systematic uncertainty. Additional systematic uncertainties associated with imperfect descriptions of multitrack efficiency correlations, ionization energy loss, and hadronic interactions in the inner tracker material are negligible. Repeating the measurement on independent subsamples of data split according to data-taking time shows no evidence of residual biases. The measured differential cross sections, averaged over each p_T bin and integrated in the rapidity range $|y| < 1$, are shown in Table I and displayed in Fig. 3. Observed cross sections are compatible with those predicted in recent calculations [14] and with those determined in early Run

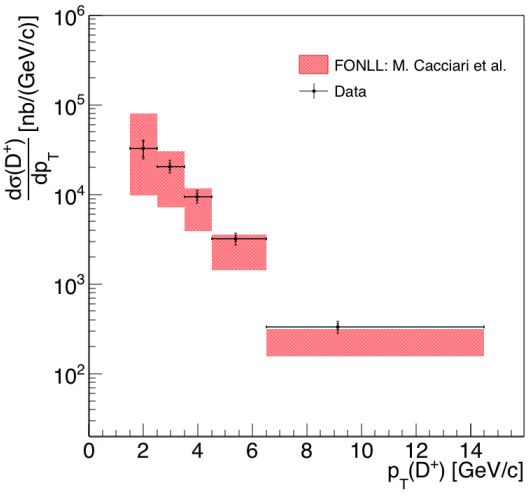

FIG. 3: Differential cross section as a function of p_T for primary D^+ mesons with $p_T > 1.5$ GeV/c, compared with predictions from Ref. [14]. In each bin, the measurement point is displayed at the "effective p_T" value at which the cross section equals the predicted p_T-averaged value over that bin. The effective-p_T values are determined using Ref. [14] and listed in Table I.

II using an independent data set [5].

p_T range (GeV/c)	Eff. p_T (GeV/c)	$d\sigma(D^+, \|y\| < 1)/dp_T$ (μb/GeV/c)	$\sigma_i(D^+, \|y\| < 1)$ (μb)
$1.5 - 2.5$	1.99	$32.7 \pm 6.5 \pm 4.2$	$32.7 \pm 6.5 \pm 4.2$
$2.5 - 3.5$	2.97	$20.6 \pm 1.8 \pm 2.7$	$20.6 \pm 1.8 \pm 2.7$
$3.5 - 4.5$	3.97	$9.50 \pm 0.84 \pm 1.2$	$9.50 \pm 0.84 \pm 1.2$
$4.5 - 6.5$	5.37	$3.23 \pm 0.26 \pm 0.42$	$6.46 \pm 0.52 \pm 0.84$
$6.5 - 14.5$	9.14	$0.34 \pm 0.04 \pm 0.04$	$2.69 \pm 0.22 \pm 0.35$

TABLE I: Results for D^+ meson cross sections. All cross-section values are integrated over the range $|y| < 1$. The second column lists the "effective p_T" values at which the point-value of cross section equals the predicted p_T-averaged value over the bin, as determined using Ref. [14]. Values in the third column are averaged over each p_T bin. The first contribution to the uncertainties is statistical, the second systematic.

The total cross section, obtained by summing over all p_T bins, is $71.9 \pm 6.8 \pm 9.3$ μb, where the first contribution to the uncertainty is statistical and the second systematic.

In summary, we report on a measurement of D^+-meson production cross-section as a function of transverse momentum in proton-antiproton collisions at 1.96 TeV center-of-mass energy, using the full data set collected by the CDF experiment in Tevatron Run II, and corresponding to 10 fb^{-1} of integrated luminosity. We use $D^+ \to K^-\pi^+\pi^+$ decays with transverse-momenta down to 1.5 GeV/c fully reconstructed in the central rapidity region $|y| < 1$. The differential cross section is averaged in each p_T bin and integrated over the D^+ rapidity interval $|y| < 1$. The total cross section is $\sigma(D^+, 1.5 < p_T < 14.5 \text{ GeV}/c, |y| < 1) = 71.9 \pm 6.8(\text{stat}) \pm 9.3(\text{syst})$ μb. The result is unique in that it probes strong-interaction dynamics in a range unexplored in charm production from proton-antiproton collisions. The results agree with earlier determinations at higher momenta [5]. While the measurements lie within the band of theoretical uncertainty, there is a systematic variation suggesting that the shape of the theoretical cross section as a function of transverse momentum can benefit by further refinement taking account these results.

ACKNOWLEDGMENTS

We thank the Fermilab staff and the technical staffs of the participating institutions for their vital contributions. This work was supported by the U.S. Department of Energy and National Science Foundation; the Italian Istituto

Nazionale di Fisica Nucleare; the Ministry of Education, Culture, Sports, Science and Technology of Japan; the Natural Sciences and Engineering Research Council of Canada; the National Science Council of the Republic of China; the Swiss National Science Foundation; the A.P. Sloan Foundation; the Bundesministerium fuer Bildung und Forschung, Germany; the Korean Science and Engineering Foundation and the Korean Research Foundation; the Particle Physics and Astronomy Research Council and the Royal Society, UK; the Russian Foundation for Basic Research; the Comision Interministerial de Ciencia y Tecnologia, Spain; and in part by the European Community's Human Potential Programme under contract HPRN-CT-20002, Probe for New Physics.

A. Public plots

We report in Figures 4 -21 the public plots for this analysis.

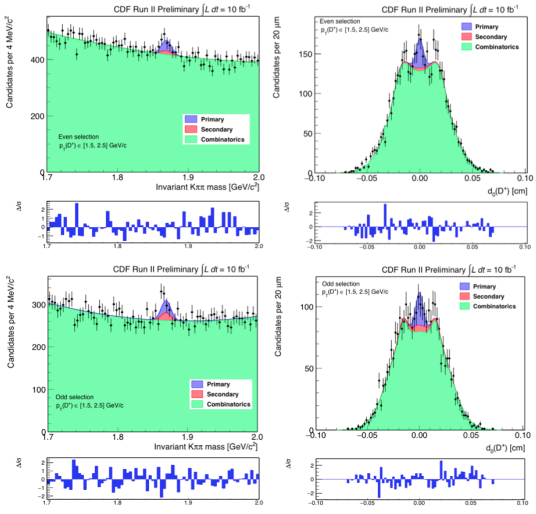

FIG. 4: Projections for even and odd events of the two-dimensional fits in the (m, d_0)-space for $p_T(D^+)$ in 1.5-2.5 GeV/c. The impact-parameter projections are for events in the mass range within three sigma of the D^+ peak value.

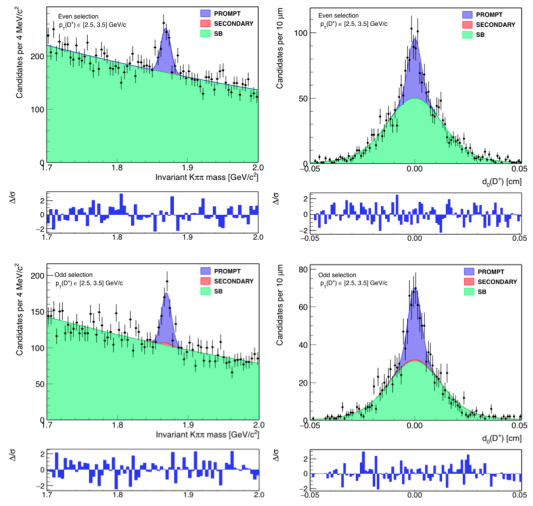

FIG. 5: Projections for even and odd events of the two-dimensional fits in the (m, d_0)-space for $p_T(D^+)$ in 2.5-3.5 GeV/c. The impact-parameter projections are for events in the mass range within three sigma of the D^+ peak value.

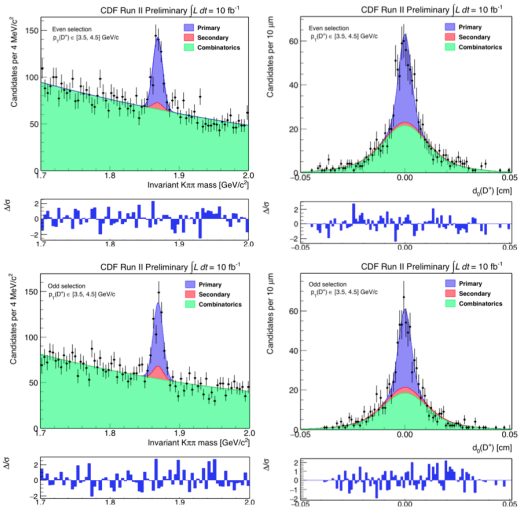

FIG. 6: Projections for even and odd events of the two-dimensional fits in the (m, d_0)-space for $p_T(D^+)$ in 3.5-4.5 GeV/c. The impact-parameter projections are for events in the mass range within three sigma of the D^+ peak value.

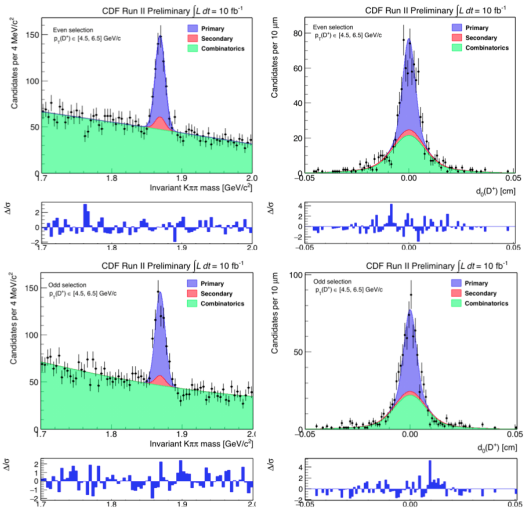

FIG. 7: Projections for even and odd events of the two-dimensional fits in the (m, d_0)-space for $p_T(D^+)$ in 4.5-6.5 GeV/c. The impact-parameter projections are for events in the mass range within three sigma of the D^+ peak value.

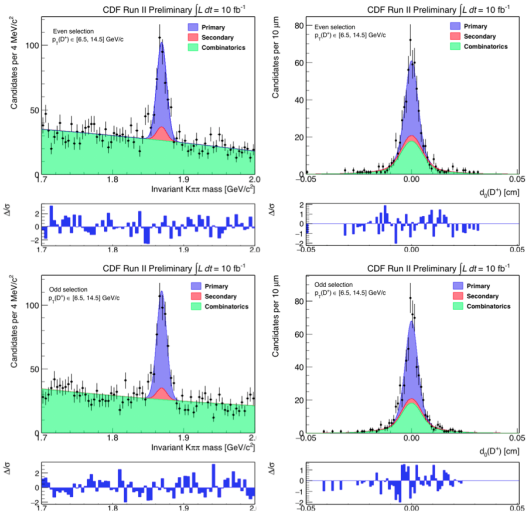

FIG. 8: Projections for even and odd events of the two-dimensional fits in the (m, d_0)-space for $p_T(D^+)$ in 6.5-14.5 GeV/c. The impact-parameter projections are for events in the mass range within three sigma of the D^+ peak value.

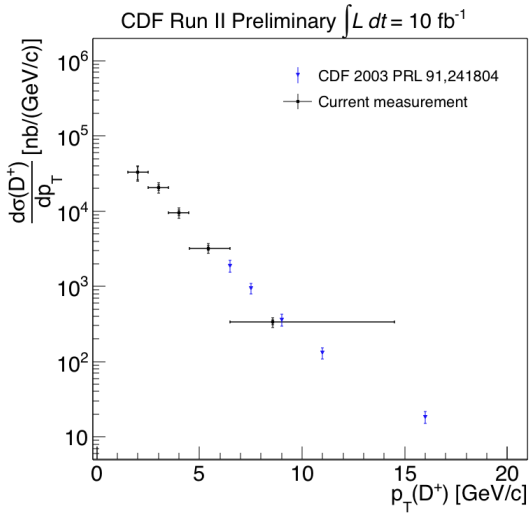

FIG. 9: D^+ production cross section as a function of $p_T(D^+)$ bins for both the current and 2003 CDF results. The current measurement is averaged in p_T-bins and integrated over $|y|$ <1, while the 2003 result is a p_T-point cross section and and integrated over $|y|$ <1. For the current result the measurement point is displayed at the mean p_T point of the bin.

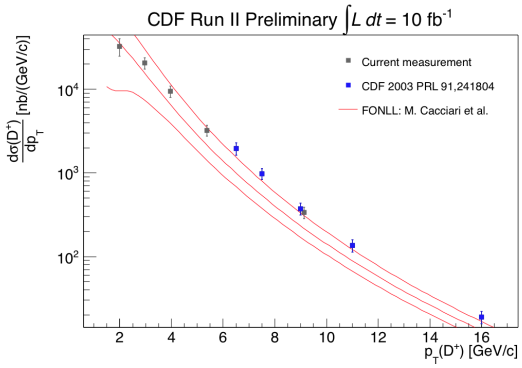

FIG. 10: D^+ production cross section as a function of $p_T(D^+)$ bins for both the current and 2003 CDF results after the theory scaling. For the current result the measurement point is displayed at the p_T point-value at which the cross section equals the predicted value of the p_T-averaged cross-section. The point values are 1.99, 2.97, 3.97, 5.37, and 9.14 GeV/c, as determined using the theoretical prediction.

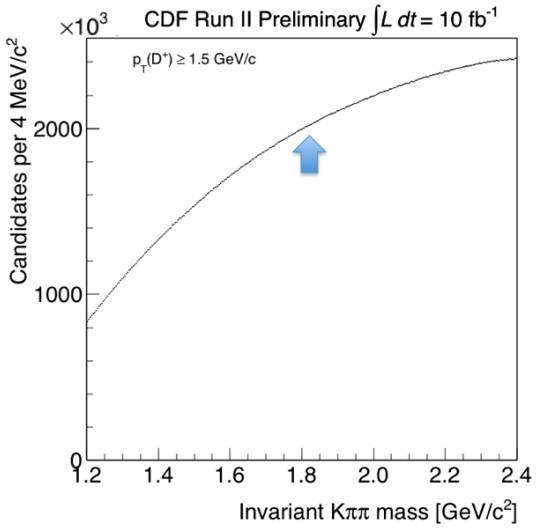

FIG. 11: Invariant $K\pi\pi$ mass before the optimization.

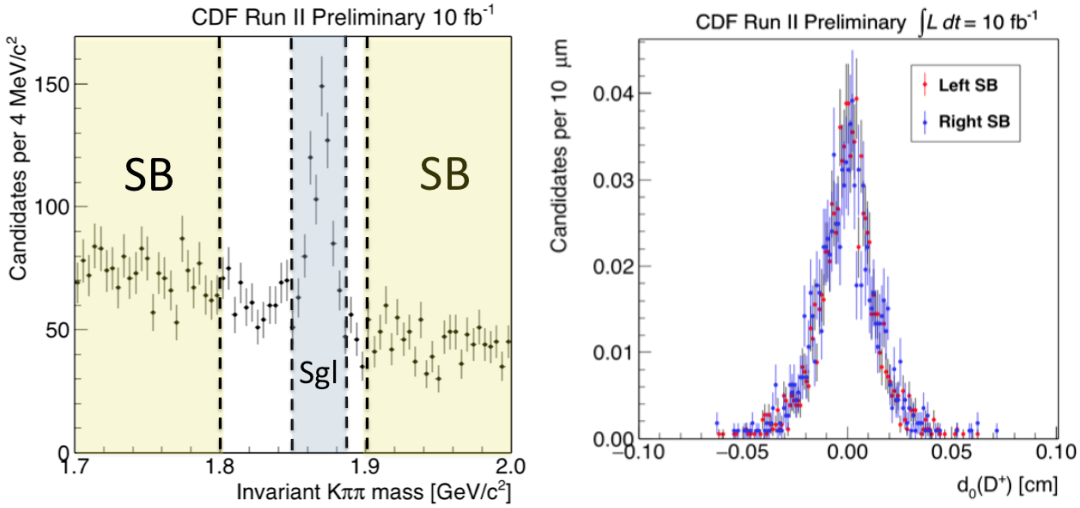

FIG. 12: Signal (left) and sidebands (right) defintion.

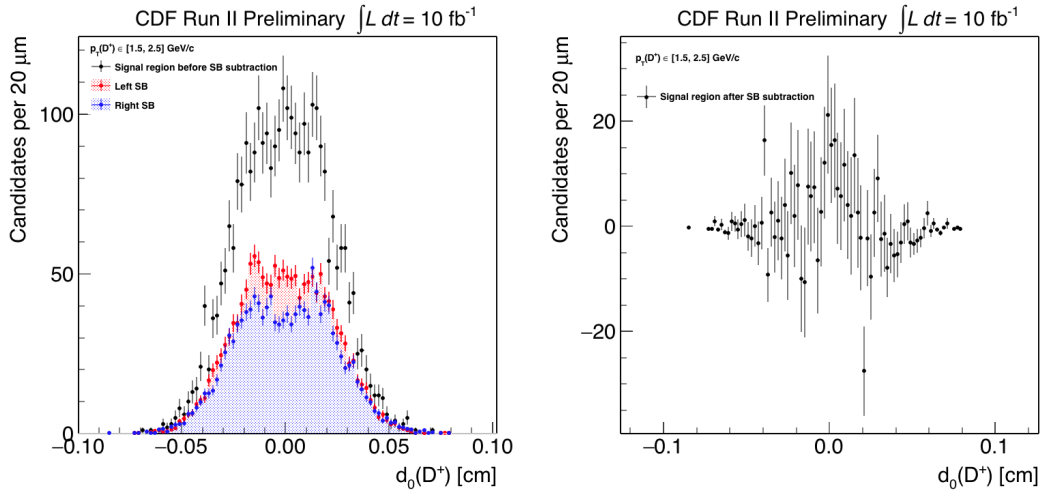

FIG. 13: Impact-parameter distribution before (left) and after (right) the sidebands subtraction for $p_T(D^+)$ in 1.5-2.5 GeV/c.

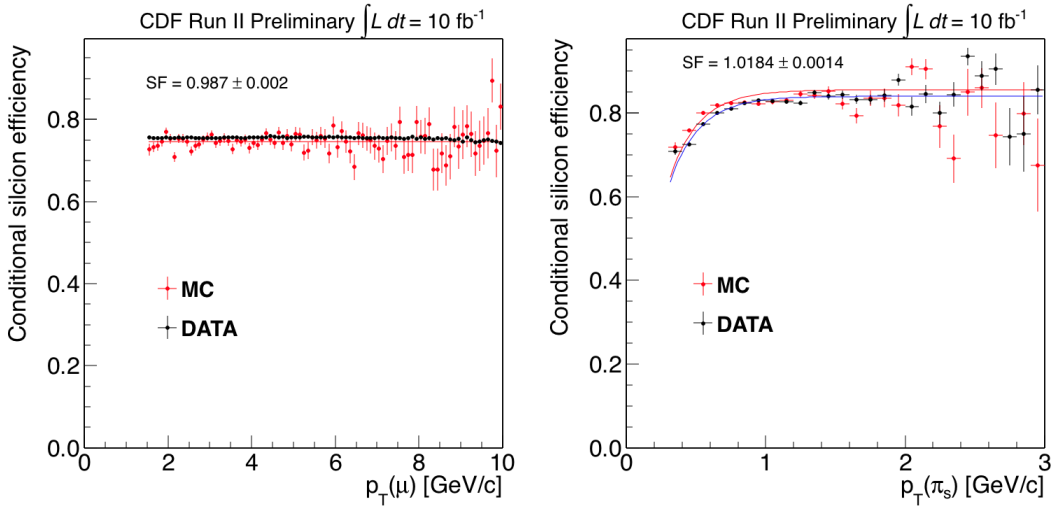

FIG. 14: Conditional-silicon efficiency in both data and MC for the J/ψ (left) and π_{soft} (right) sample.

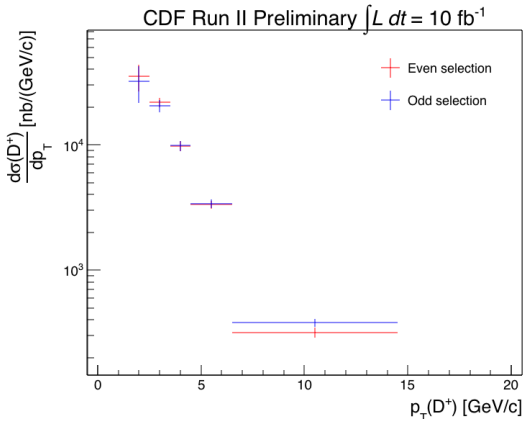

FIG. 15: Production cross section for even and odd subsamples.

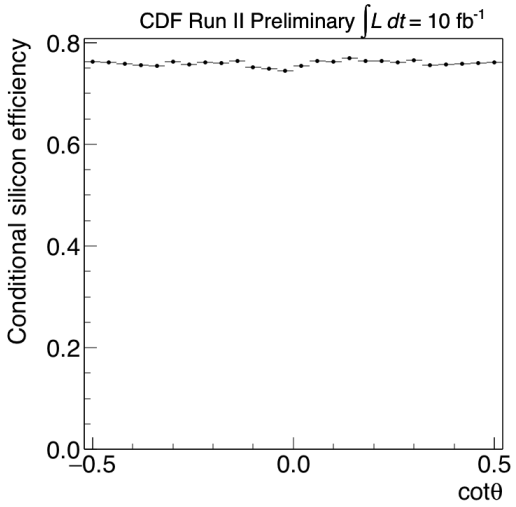

FIG. 16: Conditional-silicon efficiency as a function of cotθ for the J/ψ sample.

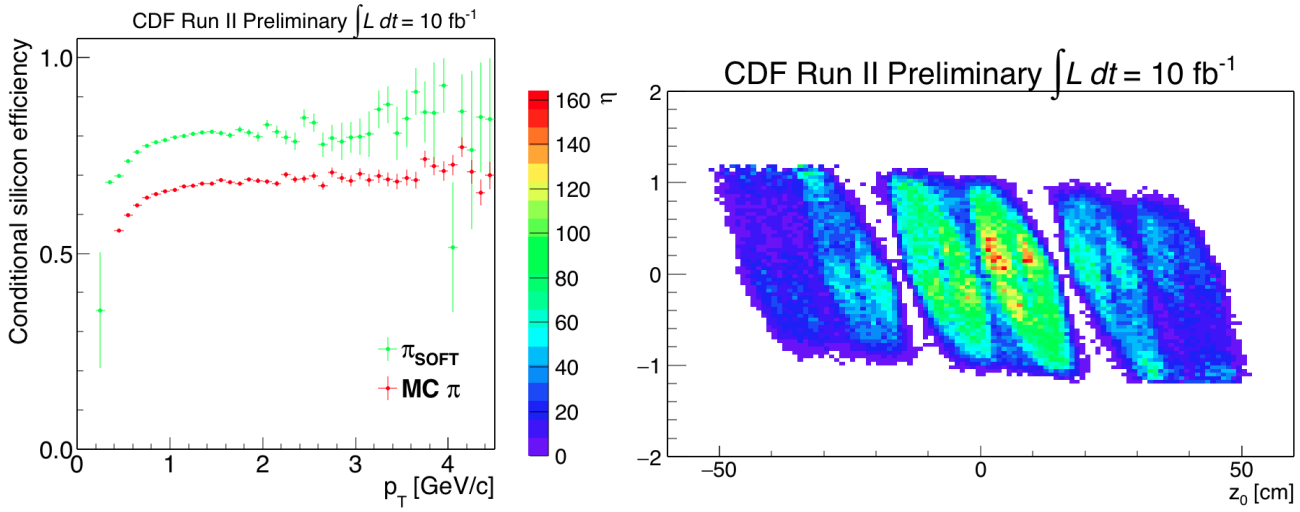

FIG. 17: Conditional-silicon efficiency for π in D^+-MC and in D^*-data (left). (η,z_0)-map for the π_{soft} dataset (right).

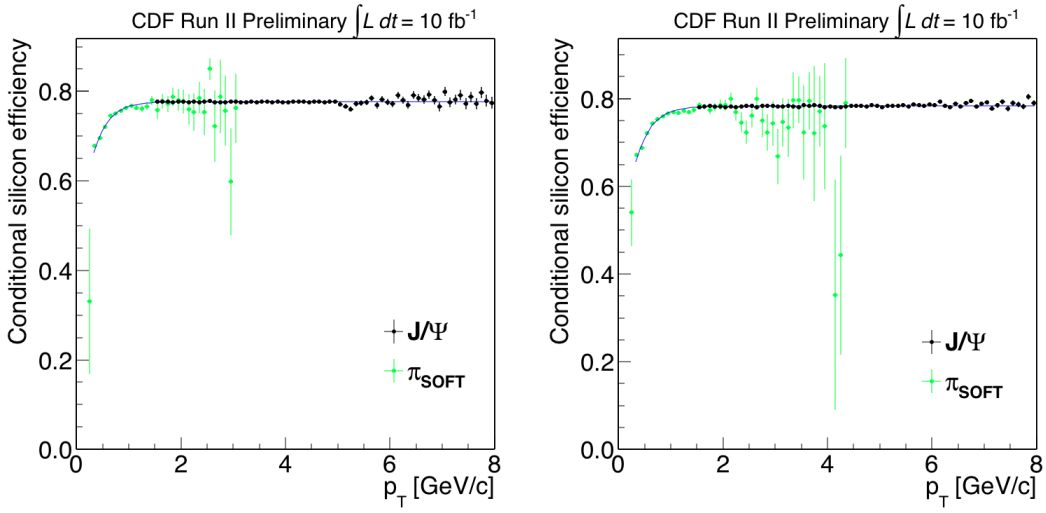

FIG. 18: Fit to the p_T-efficiency of the J/ψ and π_{soft} for the first (left) and second (right) time periods.

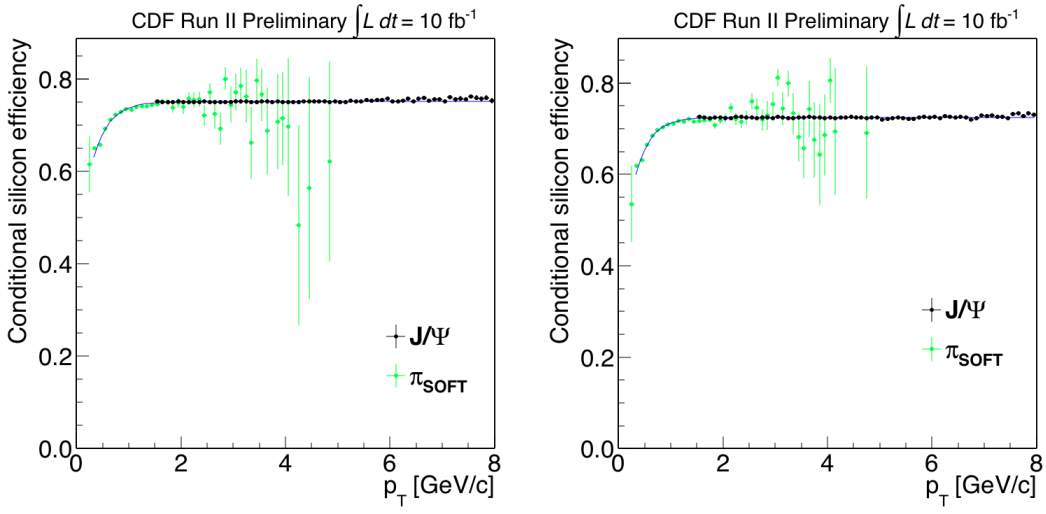

FIG. 19: Fit to the p_T-efficiency of the J/ψ and π_{soft} for the third (left) and fourth (right) time periods.

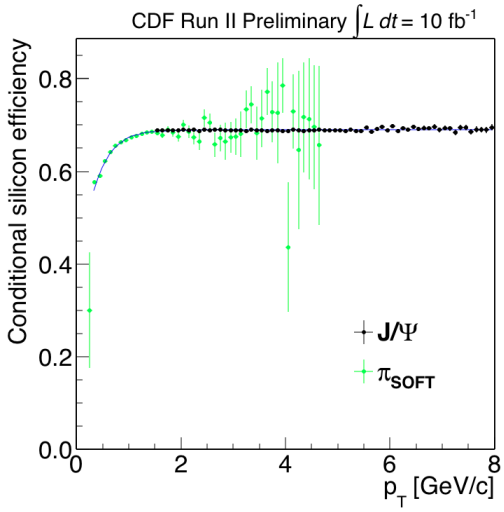

FIG. 20: Fit to the p_T-efficiency of the J/ψ and π_{soft} for the fifth time period.

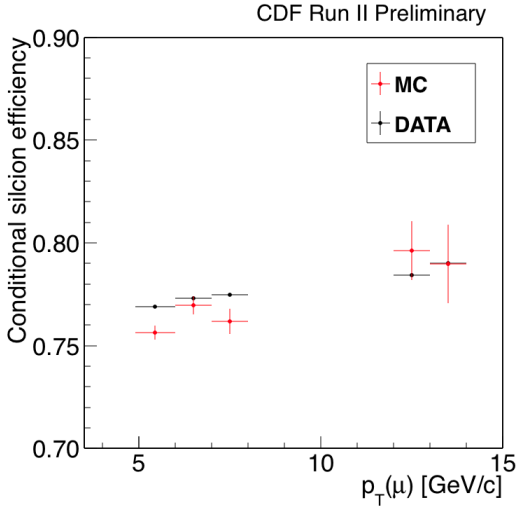

FIG. 21: Correlation study in both MC and data for the J/ψ sample: conditional silicon efficiency for the second muon when the first one is already detected by the COT.

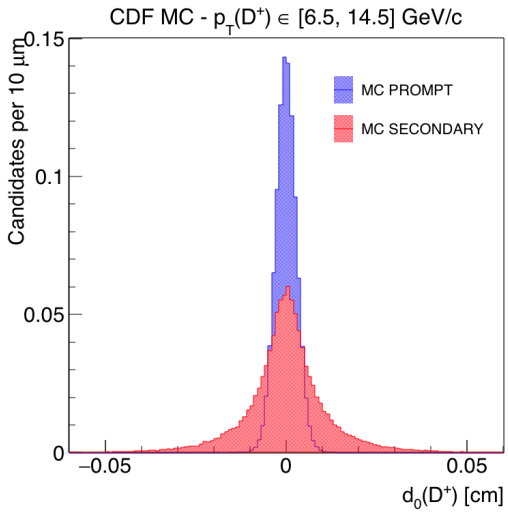

FIG. 22: Impact-parameter distribution for prompt and secondary D^+ in simulated samples for $6.5 < p_T(D^+) < 14.5$ GeV/c.

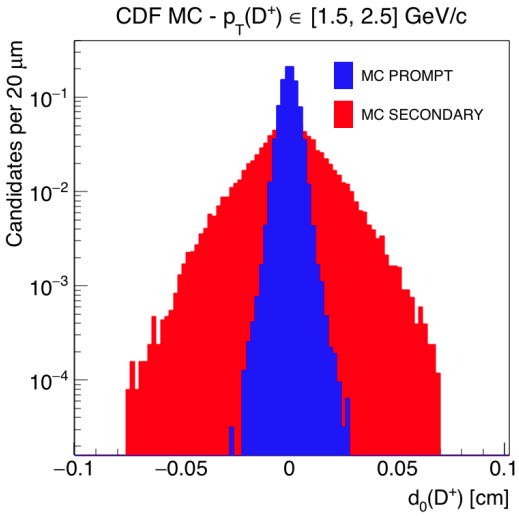

FIG. 23: Impact-parameter distribution for prompt and secondary D^+ in simulated samples for $1.5 < p_T(D^+) < 2.5$ GeV/c.

B. Tables

We report in Tables II-XII the public tables for this analysis.

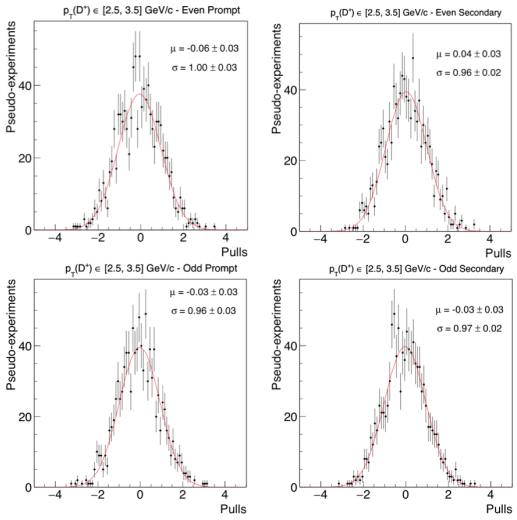

FIG. 24: Pulls study for $2.5 < p_T(D^+) < 3.5$ GeV/c. We generate an ensemble containing many pseudodata sets, each produced by randomly drawing numbers distributed according to our two-dimensional probability density function. In each, the true values for the fractions of primary and secondaries determined by the fit on data are input. Each of the pseudodata sets is fit as experimental data and the distributions of the resulting estimates are studied. As expected, they approximate Gaussian distributions centered at zero with widths compatible with the statistical uncertainty determined by the fit in data. This shows that the maximum-likelihood estimator is unbiased and has proper uncertainties.

CDF Run II Preliminary

p_T	Subsample	Primary yield	Secondary yield
1.5–2.5	Even	170 ± 40	59 ± 76
	Odd	125 ± 40	83 ± 62
2.5–3.5	Even	366 ± 27	0 ± 40
	Odd	307 ± 34	17 ± 42
3.5–4.5	Even	301 ± 28	33 ± 33
	Odd	304 ± 28	66 ± 33
4.5–6.5	Even	384 ± 29	66 ± 29
	Odd	389 ± 29	50 ± 29
6.5–13.5	Even	278 ± 24	52 ± 19
	Odd	327 ± 27	46 ± 19

TABLE II: *Results of the 2D-fit for the five $p_T(D^+)$-bins.*

[1] R. Gauld, J. Rojo, L. Rottoli, and J. Talbert, J. High Energy Phys. 11 (2015) 009 ; P. Lipari, Astropart. Phys. **1**, 195 (1993); L. Pasquali, M. Reno, and I. Sarcevic, Phys. Rev. D **59**, 034020 (1999); R. Enberg, M.H. Reno, and I. Sarcevic, Phys. Rev. D **78**, 043005 (2008); P. Gondolo, G. Ingelman, and M. Thunman, Astropart. Phys. **5**, 309 (1996); A.M. Martin, M.G. Ryskin, and A.M Stasto, Acta Phys. Polon. B**34**, 3273 (2003); M.V. Garzelli, S. Moch, and S. Sigl, J. High Energy Phys. 10 (2015) 115; G. Gelmini, P. Gondolo, and G. Varieschi, Phys. Rev. D **61**, 036005 (2000).

[2] B. Abbott *et al.* (D0 Collaboration), Phys. Lett. B **487**, 264 (2000) and D. Acosta *et al.* (CDF Collaboration), Phys. Rev. D **65**, 052005 (2002).

[3] P. Nason, S. Dawson, and R. K. Ellis, Nucl. Phys. **B327**, 49 (1989), erratum *ibid.* **B335**, 260 (1990); W. Beenakker, W. L. van Neerven, R. Meng, G. A. Schuler, and J. Smith, Nucl. Phys. **B351**, 507 (1991).

[4] J. Binnewies, B. A. Kniehl, and G. Kramer, Phys. Rev. D **58**, 034016 (1998); M. Cacciari and P. Nason, Phys. Rev. Lett. **89**, 122003 (2002); M. Cacciari, hep-ph/0407187.

[5] D. Acosta *et al.* (CDF Collaboration), Phys. Rev. Lett. **91**, 241804 (2003).

CDF Run II Preliminary

$p_T(D^+)$ [GeV/c]	Subsample	$\varepsilon_{\rm rec}(D^+)$[%]
1.5–2.5	Even	0.331 ± 0.011
	Odd	0.267 ± 0.010
2.5–3.5	Even	1.142 ± 0.026
	Odd	1.020 ± 0.025
3.5–4.5	Even	2.098 ± 0.047
	Odd	2.110 ± 0.047
4.5–6.5	Even	3.936 ± 0.073
	Odd	3.936 ± 0.073
6.5–14.5	Even	7.46 ± 0.15
	Odd	7.36 ± 0.15

TABLE III: *Reconstruction efficiency as a function of* $p_T(D^+)$.

CDF Run II Preliminary

Sample	Data-taking-time interval	SF
J/ψ	1	0.969 ± 0.007
J/ψ	2	0.985 ± 0.007
J/ψ	3	0.995 ± 0.003
J/ψ	4	1.037 ± 0.005
D^*	Time-integrated	1.0184 ± 0.0014

TABLE IV: *Scale factors for the control samples.*

[6] B. Abelev *et al.* (ALICE Collaboration), J. High Energy Phys. 01 (2012) 128; Phys. Lett. B **718**, 279 (2012); and J. High Energy Phys. 07 (2012) 191; R. Aaji *et al.* (LHCb Collaboration), Nucl. Phys. **B871**, 1 (2013) and J. High Energy Phys. 03 (2016) 159.

[7] We use the average of the inelastic cross sections reported in F. Abe *et al.* (CDF Collaboration), Phys. Rev. D **50**, 5535 (1994) and C. Avila *et al.* (E811 Collaboration), Phys. Lett. B **445**, 419 (1999).

[8] K. A. Olive *et al.* (Particle Data Group), Chin. Phys. C **38**, 090001 (2014) and 2015 online update.

[9] R. Blair *et al.* (CDF Collaboration), FERMILAB-PUB-96-390-E and T. Aaltonen *et al.* (CDF Collaboration), Phys. Rev. **D** 012009 (2012).

[10] A. Sill, Nucl. Instrum. Meth. A **447**, 1 (2000).

[11] T. Affolder *et al.*, Nucl. Instrum. Methods, **A** 526, 249 (2004).

[12] S. Klimenko, J. Konigsberg, and T.M. Liss, Report No. Fermilab-FN-0741, 2003 (unpublished); D. Acosta *et al.*, Nucl. Instrum. Meth. A **494**, 57 (2002).

[13] L. Marchese, Master's thesis, University of Naples Federico II, FERMILAB-MASTERS-2014-01 (2014).

[14] We use the predictions from the calculations at next-to-leading order in the strong-interaction coupling and next-to-leading theshold logarithm by M. Cacciari and P. Nason, J. High Energy Phys. 09 (2003) 006 and updates at `www.lpthe.jussieu.fr/ cacciari/fonll/fonllform.html`

CDF Run II Preliminary

$p_T(D^+)$ [GeV/c]	$\sigma^{\rm sys}_{L_{\rm trig}}$ [%]	$\sigma^{\rm sys}_{\rm shape}$ [%]	$\sigma^{\rm sys}_{\varepsilon_{\rm trig}}$ [%]	$\sigma^{\rm sys}_{\varepsilon_{\rm rec}}$ [%]	$\mathcal{B}(D^+ \to K^-\pi^+\pi^+)$ [%]	$\sigma^{\rm sys}_{\rm tot}$ [%]
1.5–2.5	5.8	1.2(1.1)	0.17	11.5	0.24	13
2.5–3.5	5.8	1.3(1.4)	0.17	11.5	0.24	13
3.5–4.5	5.8	0.9(1.1)	0.17	11.5	0.24	13
4.5–6.5	5.8	1.5(1.3)	0.17	11.5	0.24	13
6.5–14.5	5.8	1.1(1.3)	0.17	11.5	0.24	13

TABLE V: *Summary of systematic uncertainties. When parentheses are present, the number in (out of) parenthesis refer to the contribution to the even (odd) sample.*

CDF Run II Preliminary

$p_T(D^+)$ [GeV/c]	CF
[1.5; 2.5]	0.97 ± 0.09
[2.5; 3.5]	0.96 ± 0.09
[3.5; 4.5]	0.96 ± 0.09
[4.5; 6.5]	0.94 ± 0.08
[6.5; 14.5]	0.94 ± 0.09

TABLE VI: *Correction factors as a function of $p_T(D^+)$.*

CDF Run II Preliminary

$p_T(D^+)[GeV/c]$	Subsample	ε_{MC}[%]	ε_{corr}[%]	CF
[1.5; 2.5]	Even	0.331 ± 0.011	0.321 ± 0.032	0.97 ± 0.09
	Odd	0.267 ± 0.010	0.259 ± 0.026	
[2.5; 3.5]	Even	1.142 ± 0.026	1.10 ± 0.10	0.96 ± 0.09
	Odd	1.020 ± 0.025	0.98 ± 0.10	
[3.5; 4.5]	Even	2.098 ± 0.047	2.01 ± 0.19	0.96 ± 0.09
	Odd	2.110 ± 0.047	2.03 ± 0.19	
[4.5; 6.5]	Even	3.936 ± 0.073	3.70 ± 0.32	0.94 ± 0.08
	Odd	3.936 ± 0.073	3.70 ± 0.32	
[6.5; 14.5]	Even	7.46 ± 0.15	7.01 ± 0.69	0.94 ± 0.09
	Odd	7.36 ± 0.15	6.92 ± 0.68	

TABLE VII: *Reconstruction efficiency as a function of $p_T(D^+)$.*

CDF Run II Preliminary

$p_T(D^+)$ [GeV/c]	$d\sigma/dp_T(D^-)$ [nb/(GeV/c)]	$d\sigma/dp_T(D^+)$ [nb/(GeV/c)]
2.5–3.5	20 600 ± 2 200	24 040 ± 3 100
3.5–4.5	10 200 ± 1 200	9 900 ± 1 100
4.5–6.5	3 100 ± 304	3 700 ± 360
6.5–14.5	383 ± 38	384 ± 40

TABLE VIII: *Differential cross-section results for D^- and D^+ separately.*

CDF Run II Preliminary

$p_T(D^+)$ [GeV/c]	Subsample	$d\sigma/dp_T(D^+)$ [nb/(GeV/c)]
2.5–3.5	ZB	20 200 ± 2 500
	MB	20 100 ± 1 900
3.5–4.5	ZB	9 900 ± 1 100
	MB	9 200 ± 950
4.5–6.5	ZB	3 220 ± 314
	MB	3 226 ± 298
6.5–14.5	ZB	315 ± 34
	MB	351± 33

TABLE IX: *Differential cross-section results for ZB and MB samples.*

CDF Run II Preliminary

$p_T(D^+)$ [GeV/c]	Current meas.[nb/(GeV/c)]	Theory	Current Data/Theory ratio
1.5–2.5	32 700±7 509	36 009±25 847	0.91±0.69
2.5–3.5	20 600±2 975	15 565±14 663	1.32±1.27
3.5–4.5	9 500±1 378	6 538±5 070	1.45±1.15
4.5–6.5	3 230±453	2 176±1 378	1.48±0.97
6.5–14.5	336±47	218±99	1.54±0.74

TABLE X: *Present CDF differential cross-section measurement compared to the theoretical prediction.*

CDF Run II Preliminary

$p_T(D^+)$ [GeV/c]	2003 meas.[nb/(GeV/c)]*	Theory	2003 Data/Theory ratio
6–7	1 886±309	997±541	1.89±1.07
7–8	948±143	537±259	1.77±0.89
8–10	361±57	233±99	1.54±0.70
10–12	131±22	89±32	1.47±0.59
12–20	18.3±3.0	13.0±3.6	1.40±0.46

**scaled to take into account the current value of the BR = 9.46 ± 0.24 %

TABLE XI: *Previously published CDF differential cross-section measurement compared to the theoretical prediction. We have scaled the previous measurement to take into account the new value of the BR, as reported by the PDG.*

CDF Run II Preliminary

Current <Data/Theory ratio>	2003 <Data/Theory ratio>	Δ/σ
1.29±0.40	1.52±0.29	0.47

TABLE XII: *Comparison between the previous and the present CDF measurements.*